European Association for the Development of Renewable Energies, Environment and Power Quality (EA4EPQ)

International Conference on Renewable Energies and Power Quality (ICREPQ'12)
Santiago de Compostela (Spain), 28th to 30th March, 2012

A Study of Shunt Active Power Filters Applied to Three-Phase Four-Wire Systems

E. J. Acordi, L. B. G. Campanhol, S. A. O. Silva, C. B. Nascimento and A. Goedtel

Department of Electrical Engineering
Federal Technological University of Paraná - UTFPR
Av. Alberto Carazzai, 1640, CEP 86300-000 Cornélio Procópio (Brazil)
Phone: +55 (43) 3520-4000, Fax: +55 (43) 3520-4010
e-mail: edson.acordi@ifpr.edu.br, leo_campanhol@hotmail.com, augus@utfpr.edu.br, claudinor@utfpr.edu.br, agoedtel@utfpr.edu.br

Abstract. This work presents a study of shunt active power filters (APFs), which are implemented by means of both four-legs and three full-bridge voltage source inverter (VSI) topologies. These topologies are applied in three-phase four-wire systems for reactive power compensation and harmonic current suppression generated by nonlinear loads. The compensation reference currents used in both APFs are extracted from the synchronous reference frame (SRF) based controllers. A mathematical analysis of the four-legs and the three full-bridge topologies are presented in order to obtain the model in state space and the transfer functions of each system, allowing to set the proportional-integral (PI) gains used in the current controllers. Simulation results are presented in order to evaluate the performance of the APFs approaches.

Key words

Harmonic Suppression, Reactive Power Compensation, Power Quality, Shunt Active Power Filters.

1. Introduction

Nowadays harmonic pollution has risen significantly in the power supply system due to the increasing use of nonlinear loads, such as switching power supplies, inverters, single-phase and three-phase rectifiers, among others, being these used in industrial, commercial and residential applications. These loads have contributed for the generation of a great content of reactive and harmonics, which are responsible by the changing of the sinusoidal utility voltage characteristics, as well the currents drained from the power system, contributing to power quality (PQ) degradation. Besides, PQ problems arise when nonlinear single-phase loads are connected to three-phase, four-wire systems. Even if these loads are perfectly balanced, harmonic currents circulate through the neutral conductor, which will always occur due to the existence of zero sequence components. The amplitudes of these currents may exceed those of the individual phase current, which can cause damage to the neutral conductor and to the transformers where the loads are connected [1-3].

An alternative method to solve or minimize these problems is the use of shunt active power filters (APFs), applied in single-phase and three-phase three-wire and four-wire systems. APFs are used to inject in the line, compensation currents in order to cancel harmonics and/or reactive components of the load currents. For three-phase four-wire systems, depending on the control strategies adopted, the APF can control each phase independently. Thus, it is possible to compensate all the harmonic and reactive current components. In this case, the compensation of the unbalanced load is not taken into account [7].

This paper presents a study of two APF topologies, which are applied to three-phase four-wire systems, such as the four-legs (F-L) [3-6], and three full-bridge (3F-B) [3, 7-9], as shown in Fig. 1 and Fig. 2, respectively. Both are used for harmonic current suppression, reactive power compensation and/or load unbalance compensation.

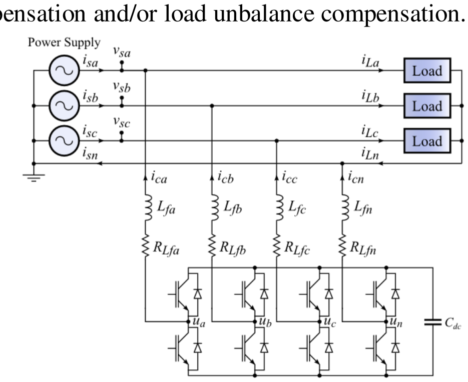

Fig. 1. Four-Legs (F-L) APF topology.

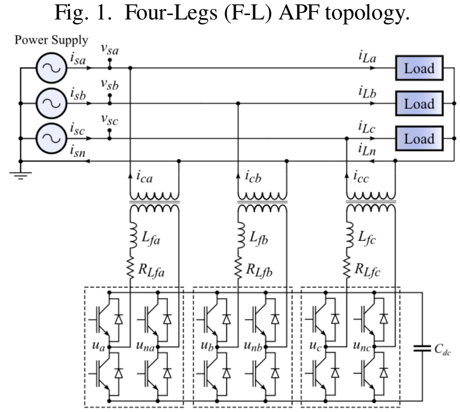

Fig. 2. Three Full-Bridge (3F-B) APF topology.

The algorithms used to extract the three-phase compensation reference currents are based on the SRF [10]. While the F-L topology uses the three-phase SRF-based algorithm, the 3F-B uses the single-phase one. Mathematical analyses of the two topologies are developed in order to present the method used to obtain the state space equation and the transfer functions that represent the physical systems. Simulation results are presented to evaluate the performance of the APFs studied, which are modulated using the space vector modulation (SVM) [11, 12].

2. SRF-Based algorithms

In this work, SRF-based algorithms are used to extract the three-phase compensation reference currents ($i^*_{ca}, i^*_{cb}, i^*_{cc}$) used by the APFs.

The F-L topology shown in Fig. 1 uses the traditional SRF-based algorithm ($dq0$-axes). Despite the proportional-integral (PI) controllers of the system have been designed to operate in the synchronous rotating reference frame, the SVM is performed in the stationary reference frame ($\alpha\beta 0$-axes) [11, 12]. On the other hand, the 3F-B shown in Fig. 2 utilizes the SRF-based algorithm adapted for single-phase systems. Thus, the control of this structure can be designed to operate independently in each phase of the three-phase system.

A. SRF-Based Algorithm Applied to F-L Topology

The three-phase SRF-based algorithm, used in the F-L topology for harmonic suppression, reactive and load unbalance compensation is shown in Figure 3.

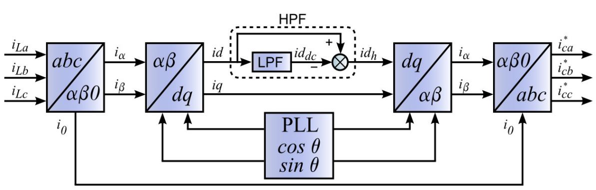

Fig. 3. Block diagram of the SRF-based algorithm.

In this method, the load currents (i_{La}, i_{Lb}, i_{Lc}) are measured and transformed from a three-phase stationary reference frame (*abc*) into two-phase stationary reference frame ($\alpha\beta 0$), as given by (1).

$$\begin{bmatrix} i_\alpha \\ i_\beta \\ i_0 \end{bmatrix} = \sqrt{\frac{2}{3}} \begin{bmatrix} 1 & -\frac{1}{2} & -\frac{1}{2} \\ 0 & \frac{\sqrt{3}}{2} & -\frac{\sqrt{3}}{2} \\ \frac{1}{\sqrt{2}} & \frac{1}{\sqrt{2}} & \frac{1}{\sqrt{2}} \end{bmatrix} \begin{bmatrix} i_{La} \\ i_{Lb} \\ i_{Lc} \end{bmatrix} \tag{1}$$

Thus, the current quantities of the $\alpha\beta$-axes can be transformed into two-phase synchronous reference frame (dq-axes) using (2), where $\cos\theta$ and $\sin\theta$ are the synchronous unit vectors obtained from any phase-locked loop (PLL) system.

$$\begin{bmatrix} id \\ iq \end{bmatrix} = \begin{bmatrix} \cos\theta & \sin\theta \\ -\sin\theta & \cos\theta \end{bmatrix} \begin{bmatrix} i_\alpha \\ i_\beta \end{bmatrix} \tag{2}$$

Now, the dq currents are composed by dc and ac parts. The dc part represents the fundamental load currents (active and reactive), and the ac part represents the harmonic components that can be extracted using a high pass filter (HPF), as implemented in Fig. 3. The d-axis current id represents the sum of the fundamental active current (id_{dc}) and a parcel of the load harmonic current (id_h). By filtering id, the current id_{dc} (Fig. 3) is obtained, which represents the fundamental active load currents in the synchronous frame. Thus, the ac component id_h is obtained by subtracting the id_{dc} component of the total current in d-axis (id), which allow to achieve the harmonic parcel of the load current. In the synchronous frame the q-axis current (iq) represents the sum of the fundamental reactive load currents and part of the load harmonic currents. It can be totally used to calculate the reference compensation currents.

The inverse transformation from the two-phase synchronous reference frame dq into two-phase stationary frame $\alpha\beta$ is obtained by (3).

$$\begin{bmatrix} i_\alpha \\ i_\beta \end{bmatrix} = \begin{bmatrix} \cos\theta & -\sin\theta \\ \sin\theta & \cos\theta \end{bmatrix} \begin{bmatrix} id_h \\ iq \end{bmatrix} \tag{3}$$

The inverse transformation from stationary frame $\alpha\beta 0$ into three-phase stationary frame abc is shown by (4), in which the compensation references currents are obtained.

$$\begin{bmatrix} i^*_{ca} \\ i^*_{cb} \\ i^*_{cc} \end{bmatrix} = \left[T_{abc}\right] \begin{bmatrix} i_\alpha \\ i_\beta \\ i_0 \end{bmatrix} \tag{4}$$

where:

$$\left[T_{abc}\right] = \sqrt{\frac{2}{3}} \begin{bmatrix} 1 & 0 & \frac{1}{\sqrt{2}} \\ -\frac{1}{2} & \frac{\sqrt{3}}{2} & \frac{1}{\sqrt{2}} \\ -\frac{1}{2} & -\frac{\sqrt{3}}{2} & \frac{1}{\sqrt{2}} \end{bmatrix} \tag{5}$$

B. SRF-Based Algorithm Applied to 3F-B Topology

The SRF-based algorithm used in the 3F-B topology is shown in Figure 4.

The first strategy adopted to control the 3F-B topology is to treat each phase independently as a fictitious three-phase system. Thus, only load harmonic suppression and reactive power compensation are carried out and the load unbalanced current compensation is not taken into account.

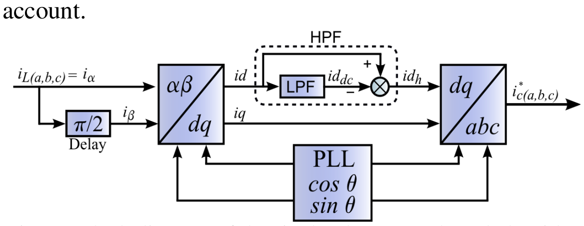

Fig. 4. Block diagram of the single-phase SRF-based algorithm.

Thereby, measuring the three-phase load currents (i_{La}, i_{Lb}, i_{Lc}), it is possible to obtain three fictitious stationary reference frame in $\alpha\beta$-axes ($i'_{\alpha_{a,b,c}}$, $i'_{\beta_{a,b,c}}$). The acquired load current is treated as the α-coordinate of the fictitious $\alpha\beta$-axes, for instance $i'_{\alpha_a} = i_{La}$. Subsequently, $i'_{\alpha_{a,b,c}}$ has a $\pi/2$ radian phase delay producing the fictitious β-coordinate ($i'_{\beta_{a,b,c}}$). Therefore, three fictitious two-phase systems, represented by (6), are obtained in the $\alpha\beta$-axes, and the transformation from the stationary three-phase frame *abc* into stationary system $\alpha\beta 0$ is not necessary. Thus, only the transformation from $\alpha\beta$-axes into dq-axes is taken into account, as given by (2).

$$\begin{bmatrix} i'_{\alpha_{a,b,c}} \\ i'_{\beta_{a,b,c}} \end{bmatrix} = \begin{bmatrix} i_{L_{a,b,c}}(\omega t) \\ i_{L_{a,b,c}}(\omega t - \pi/2) \end{bmatrix} \tag{6}$$

Finally, the compensation reference currents (i^*_{ca}, i^*_{cb}, i^*_{cc}) are obtained directly from dq-axes as given by (7).

$$i^*_{c_{a,b,c}} = \begin{bmatrix} \cos\theta_{a,b,c} & -\sin\theta_{a,b,c} \end{bmatrix} \begin{bmatrix} id_{h_{a,b,c}} \\ iq_{a,b,c} \end{bmatrix} \tag{7}$$

The second strategy adopted to control the 3F-B topology is shown in Fig. 5, which the compensation of the load unbalanced currents is taken into account. In this case, the input currents $i_{s_{a,b,c}}$ will be controlled to become sinusoidal and balanced.

To implement this strategy, the outputs of the LPF shown in Fig. 4, which represents the active current of each phase treated independently, are used as the input current quantities of the SRF algorithm shown in Fig. 5. Thus, the input sinusoidal and balanced reference currents $i^*_{s_{a,b,c}}$ can be obtained. Now, the compensation reference currents $i^*_{c_{a,b,c}}$ are obtained subtracting $i^*_{s_{a,b,c}}$ of $i_{L_{a,b,c}}$, as given by (8).

$$i^*_{c_{a,b,c}} = i_{L_{a,b,c}} - i^*_{s_{a,b,c}} \tag{8}$$

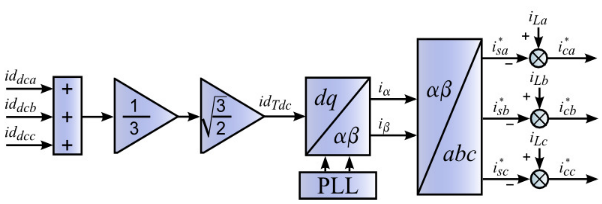

Fig. 5. Block diagram of the unbalanced load compensating.

3. Shunt APFs applied to four-wire systems

The description of the two APFs studied in this paper and their respective mathematic modeling are presented in this section.

A. Four-Legs topology

The F-L topology (Fig. 1) is implemented using four-leg full-bridge VSI converter [3-6], Thus, one of the four-leg is used to control the neutral current.

The control of F-L topology implemented is based on SRF controller. Thereby, the mathematical modeling is presented in order to obtain the state space system and the transfer functions in the *dq0* frame. To perform the modeling, all the coupling inductances and their resistances are assumed to be identical, such as $L_{fa} = L_{fb} = L_{fc} = L_{fn} = L_f$ and $R_{Lfa} = R_{Lfb} = R_{Lfc} = R_{Lfn} = R_{Lf}$. Thus, from Fig. 1, the inverter output voltages can be expressed by:

$$u_{anpwm} = R_{Lf}.i_{sa} + L_f\frac{di_{sa}}{dt} + v_{sa} + L_f\frac{di_{cn}}{dt} + R_{Lf}.i_{cn} \tag{9}$$

$$u_{bnpwm} = R_{Lf}.i_{sb} + L_f\frac{di_{sb}}{dt} + v_{sb} + L_f\frac{di_{cn}}{dt} + R_{Lf}.i_{cn} \tag{10}$$

$$u_{cnpwm} = R_{Lf}.i_{sc} + L_f\frac{di_{sc}}{dt} + v_{sc} + L_f\frac{di_{cn}}{dt} + R_{Lf}.i_{cn} \tag{11}$$

where $u_{anpwm} = u_a - u_n$, $u_{bnpwm} = u_b - u_n$ and $u_{cnpwm} = u_c - u_n$.

As $i_{sa} + i_{sb} + i_{sc} = i_{sn}$, its derivative form is given by:

$$\frac{di_{sa}}{dt} + \frac{di_{sb}}{dt} + \frac{di_{sc}}{dt} = \frac{di_{sn}}{dt} \tag{12}$$

Adding (9), (10) and (11), and using some algebraic manipulations, the following state equations can be found:

$$\frac{di_{sa}}{dt} = \frac{1}{4L_f}\left[\left(3u_{anpwm} - u_{bnpwm} - u_{cnpwm}\right) + \left(-4v_{R_{Lf}} - 3v_{sa} + v_{sb} + v_{sc}\right)\right] \tag{13}$$

$$\frac{di_{sb}}{dt} = \frac{1}{4L_f}\left[\left(-u_{anpwm} + 3u_{bnpwm} - u_{cnpwm}\right) + \left(-4v_{R_{Lf}} + v_{sa} - 3v_{sb} + v_{sc}\right)\right] \tag{14}$$

$$\frac{di_{sc}}{dt} = \frac{1}{4L_f}\left[\left(-u_{anpwm} - u_{bnpwm} + 3u_{cnpwm}\right) + \left(-4v_{R_{Lf}} + v_{sa} + v_{sb} - 3v_{sc}\right)\right] \tag{15}$$

The state-space system is defined as:

$$\dot{x}(t) = A.x(t) + B.u(t) + F.w(t) \tag{16}$$

where:

$$\dot{x}(t) = \begin{bmatrix} \frac{di_{sa}}{dt} & \frac{di_{sb}}{dt} & \frac{di_{sc}}{dt} \end{bmatrix}^T; \quad x = \begin{bmatrix} i_{sa} & i_{sb} & i_{sc} \end{bmatrix}^T;$$

$$u = \begin{bmatrix} u_{anpwm} & u_{bnpwm} & u_{cnpwm} \end{bmatrix}^T; \quad w = \begin{bmatrix} v_{sa} & v_{sb} & v_{sc} \end{bmatrix}^T.$$

Thus, using (13), (14), (15) and (16) is possible to obtain the matrices that represent the state-space model of the F-L topology into the stationary frame *abc*, as follows:

$$A = \frac{R_{Lf}}{L_f}\begin{bmatrix} -1 & 0 & 0 \\ 0 & -1 & 0 \\ 0 & 0 & -1 \end{bmatrix}, \; B = \frac{1}{4L_f}\begin{bmatrix} 3 & -1 & -1 \\ -1 & 3 & -1 \\ -1 & -1 & 3 \end{bmatrix}, \; F = \frac{1}{4L_f}\begin{bmatrix} -3 & 1 & 1 \\ 1 & -3 & 1 \\ 1 & 1 & -3 \end{bmatrix} \tag{17}$$

In order to represent (16) into the stationary frame $\alpha\beta 0$, the transformation matrix given by (5) is used. Thus, (16) can be rewritten as:

$$\begin{aligned} T_{abc}.\dot{x}_{\alpha\beta 0}(t) &= A.T_{abc}.x_{\alpha\beta 0}(t) + \\ & B.T_{abc}.u_{\alpha\beta 0}(t) + F.T_{abc}.w_{\alpha\beta 0}(t) \end{aligned} \tag{18}$$

Multiplying both sides of (18) by $\left[T_{abc}\right]^{-1}$, $\dot{x}_{\alpha\beta 0}$ is obtained as follows:

$$\dot{x}_{\alpha\beta 0}(t) = A_{\alpha\beta 0}.x_{\alpha\beta 0}(t) + B_{\alpha\beta 0}.u_{\alpha\beta 0}(t) + F_{\alpha\beta 0}.w_{\alpha\beta 0}(t) \tag{19}$$

where:

$$A_{\alpha\beta 0} = \frac{R_{Lf}}{L_f}\begin{bmatrix} -1 & 0 & 0 \\ 0 & -1 & 0 \\ 0 & 0 & -1 \end{bmatrix}, B_{\alpha\beta 0} = \frac{1}{4L_f}\begin{bmatrix} 4 & 0 & 0 \\ 0 & 4 & 0 \\ 0 & 0 & 1 \end{bmatrix},$$
$$F_{\alpha\beta 0} = \frac{1}{4L_f}\begin{bmatrix} -4 & 0 & 0 \\ 0 & -4 & 0 \\ 0 & 0 & -1 \end{bmatrix} \tag{20}$$

To represent (19) into $dq0$-axes, the transformation matrix given by (21) is used.

$$T_{dq0} = \begin{bmatrix} \cos\omega t & \sin\omega t & 0 \\ -\sin\omega t & \cos\omega t & 0 \\ 0 & 0 & 1 \end{bmatrix} \tag{21}$$

Thus, (19) can be rewritten as:

$$\begin{aligned} \left[\dot{T_{dq0}^{-1}.x_{dq0}(t)}\right] &= A_{\alpha\beta o}.T_{dq0}^{-1}.x_{dq0}(t) \\ &+ B_{\alpha\beta o}.T_{dq0}^{-1}.u_{dq0}(t) + F_{\alpha\beta o}.T_{dq0}^{-1}.w_{dq0}(t) \end{aligned} \tag{22}$$

Isolating the terms in (22), and through some manipulations, $\dot{x}_{dq0}$ is obtained as follows:

$$\dot{x}_{dq0}(t) = A_{dq0}.x_{dq0}(t) + B_{dq0}.u_{dq0}(t) + F_{dq0}.w_{dq0}(t) \tag{23}$$

where:

$$A_{dq0} = \begin{bmatrix} -\dfrac{R_{Lf}}{L_f} & \omega & 0 \\ -\omega & -\dfrac{R_{Lf}}{L_f} & 0 \\ 0 & 0 & -\dfrac{R_{Lf}}{L_f} \end{bmatrix},$$
$$B_{dq0} = \frac{1}{4L_f}\begin{bmatrix} 4 & 0 & 0 \\ 0 & 4 & 0 \\ 0 & 0 & 1 \end{bmatrix}, \; F_{dq0} = \frac{1}{4L_f}\begin{bmatrix} -4 & 0 & 0 \\ 0 & -4 & 0 \\ 0 & 0 & -1 \end{bmatrix} \tag{24}$$

The block diagram of the physical system in $dq0$-axes is shown in Fig. 6, where D_d, D_q, and D_0 are the duty cycles in the synchronous reference frame, which are obtained from the SVM, and V_{dc} is dc-bus voltage.

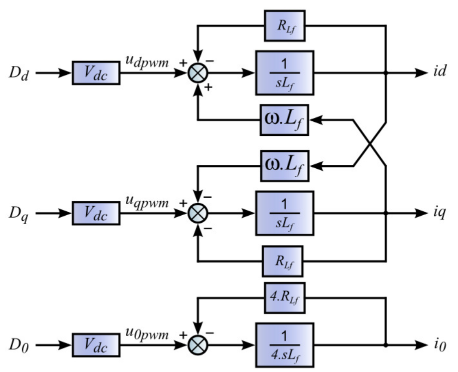

Fig. 6. Physical system model of the F-L in $dq0$ coordinates.

The cross-coupling between the direct and quadrature axes can be eliminated using the decoupled model shown in Fig. 7, where the shaded block is the decoupling term.

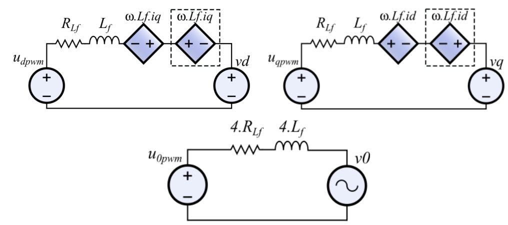

Fig. 7. Model of the decoupled system in $dq0$ coordinates.

Thus, in the synchronous $dq0$-frame, neglecting the cross-coupling, the transfer functions of the system $G_{ps(d,q)}$ and G_{ps0} are given by (25).

$$G_{ps(d,q)}(s) = \frac{1}{(R_{Lf} + s.L_f)}, \; G_{ps0}(s) = \frac{1}{4(R_{Lf} + s.L_f)} \tag{25}$$

The block diagram of the current controller is shown in Fig. 8 (a), where the PI controller is used. Thereby, the closed loop transfer functions $i_{(d,q)}(s)/i^*_{(d,q)}(s)$ and $i_0(s)/i^*_0(s)$ are obtained, respectively, as follows:

$$\frac{i_{(d,q)}(s)}{i^*_{(d,q)}(s)} = \frac{Kp_{i(d,q)}s + Ki_{i(d,q)}}{L_f.s^2 + (R_{Lf} + Kp_{i(d,q)})s + Ki_{i(d,q)}} \tag{26}$$

$$\frac{i_0(s)}{i^*_0(s)} = \frac{Kp_{i0}s + Ki_{i0}}{4L_f.s^2 + (4R_{Lf} + Kp_{i0})s + Ki_{i0}} \tag{27}$$

The details of the Current Reference Generation and Control block represented in Fig. 8a are shown in Fig. 8b.

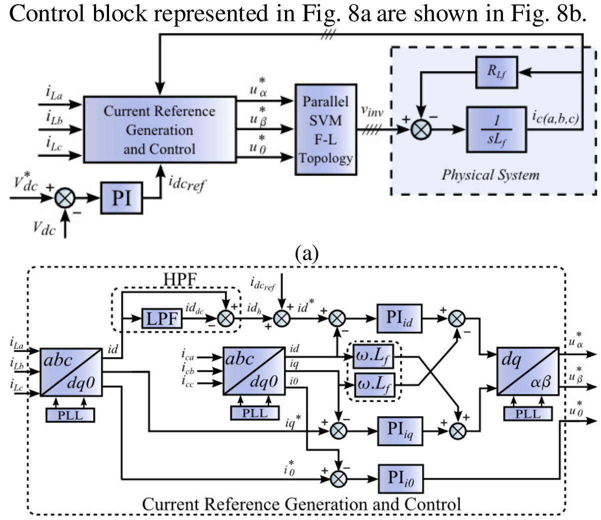

Fig. 8. (a) Block Diagram of the F-L current controller; (b) Current Reference Generation and Control details.

C. Three Full-Bridge topology

The 3F-B topology shown in Fig. 2 is implemented using three single-phase full-bridge VSI converters [3, 7-9]. The main characteristic of this topology is the independent control of the three phases. Another important aspect to be considered is that the dc-bus is reduced by a factor of $\sqrt{3}$, when it is compared with the F-L topology. Thereby, this topology could be an interesting choice for high power applications [7]. As can be seen in Fig. 2, the number of switching devices is increased when compared with the F-L topology (Fig. 1). Besides, three single-phase isolation transformers are required due to the sharing of the same dc-bus voltage.

The control of 3F-B topology is implemented into the three-phase stationary *abc*-frame, being also presented the mathematical modeling, where the transformers are assumed to be ideals and the transformation ratios of them are equal to one. Thus, through Fig. 2, the output voltage of each inverter can be written as:

$$u_{a_{napwm}} = R_{Lf}.i_{sa} + L_f \frac{di_{sa}}{dt} + v_{sa} \tag{28}$$

$$u_{b_{nbpwm}} = R_{Lf}.i_{sb} + L_f \frac{di_{sb}}{dt} + v_{sb} \tag{29}$$

$$u_{c_{ncpwm}} = R_{Lf}.i_{sc} + L_f \frac{di_{sc}}{dt} + v_{sc} \tag{30}$$

Isolating $di_{s(a,b,c)}/dt$, (31), (32) and (33) are obtained.

$$\frac{di_{sa}}{dt} = \frac{1}{L_f}\left(-R_{Lf}.i_{sa} + u_{a_{napwm}} - v_{sa}\right) \tag{31}$$

$$\frac{di_{sb}}{dt} = \frac{1}{L_f}\left(-R_{Lf}.i_{sb} + u_{b_{nbpwm}} - v_{sb}\right) \tag{32}$$

$$\frac{di_{sc}}{dt} = \frac{1}{L_f}\left(-R_{Lf}.i_{sc} + u_{c_{ncpwm}} - v_{sc}\right) \tag{33}$$

From (31), (32), (33) and (16), the matrices that represent the state-space models in the *abc*-frame are given by (34).

$$A = \frac{R_{Lf}}{L_f}\begin{bmatrix} -1 & 0 & 0 \\ 0 & -1 & 0 \\ 0 & 0 & -1 \end{bmatrix},\ B = \frac{1}{L_f}\begin{bmatrix} 1 & 0 & 0 \\ 0 & 1 & 0 \\ 0 & 0 & 1 \end{bmatrix},\quad F = \frac{1}{L_f}\begin{bmatrix} -1 & 0 & 0 \\ 0 & -1 & 0 \\ 0 & 0 & -1 \end{bmatrix} \tag{34}$$

From (34), the *abc* transfer functions of the physical system ($G_{ps(a,b,c)}$) are obtained as:

$$G_{ps(a,b,c)}(s) = \frac{1}{(R_{Lf} + L_f.s)} \tag{35}$$

The block diagram of the single-phase current controller is shown in Fig. 9, where the closed loop transfer functions $i_{c(a,b,c)}(s)/i^*_{c(a,b,c)}(s)$ are given by (36).

$$\frac{i_{c(a,b,c)}(s)}{i^*_{c(a,b,c)}(s)} = \frac{Kp_{i(a,b,c)}s + Ki_{i(a,b,c)}}{L_f.s^2 + (R_{Lf} + Kp_{i(a,b,c)})s + Ki_{i(a,b,c)}} \tag{36}$$

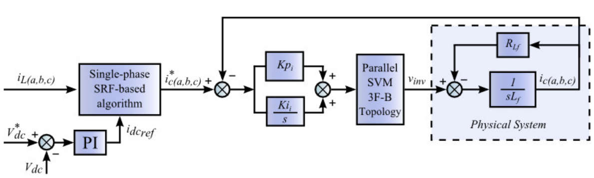

Fig. 9. Block diagram of the 3F-B current controller (per phase).

4. Simulation Results

To verify the behavior of the two topologies, they were simulated with the computational tool MATLAB/Simulink®, in which the three-phase converters operate at 20 kHz switching frequency. The simulations were performed considering a three-phase four-wire system feeding three unbalanced nonlinear loads, as shown in Fig. 10. The parameters of APFs and PI controller gains are shown in Table I.

Figure 11 shows the three-phase uncompensated loads currents (i_{La}, i_{Lb}, i_{Lc}). Figure 12 and Fig. 13 show the compensated source currents (i_{sa}, i_{sb}, i_{sc}), the neutral current (i_{sn}) and the dc-bus voltage (V_{dc}), for the F-L and 3F-B topologies, respectively. As can be noted, the APFs are performing harmonic current suppression, reactive power compensation and load unbalanced compensation.

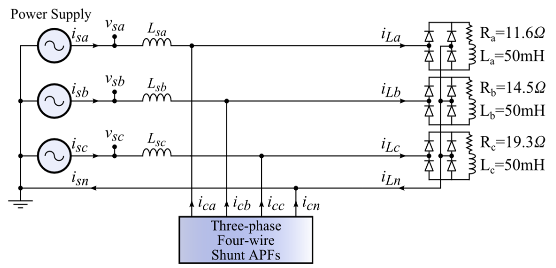

Fig. 10. Three-phase four-wire system feeding nonlinear loads.

Table I - Parameters of the shunt APFs.

Parameters	F-L	3F-B
dc-bus voltage (V_{dc})	400V	230V
dc-bus capacitor (C_{dc})	3mF	3mF
Inductor ($L_{f(a,b,c)}$)	1mH	1mH
Inductor (L_{fn})	1mH	--
PI controller parameters		
Proportional gain (current loop)	$Kp_{i(d,q)}$=31.42 Kp_{i0}=126	$Kp_{i(a,b,c)}$=31.42
Integral gain (current loop)	$Ki_{i(d,q)}$=1570 Ki_{i0}=6283	$Ki_{i(a,b,c)}$=1570
Proportional gain (dc-voltage loop)	Kp_v=0.53	Kp_v=0.55
Integral gain (dc-voltage loop)	Ki_v=36.46	Ki_v=15.50

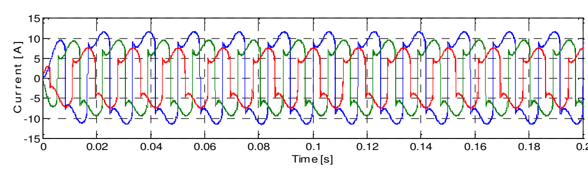

Fig. 11. Three-phase load currents: i_{La}, i_{Lb} and i_{Lc}.

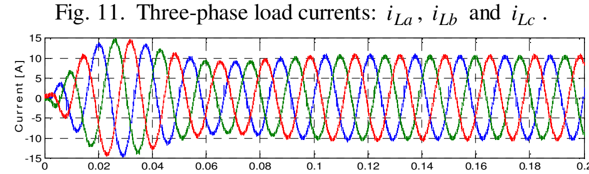

(a)

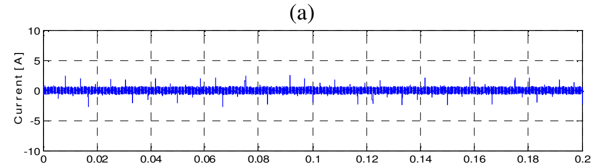

(b)

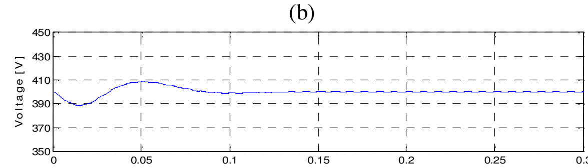

(c)

Fig. 12. F-L topology: (a) i_{sa}, i_{sb} and i_{sc}, (b) i_{sn}; (c) V_{dc}.

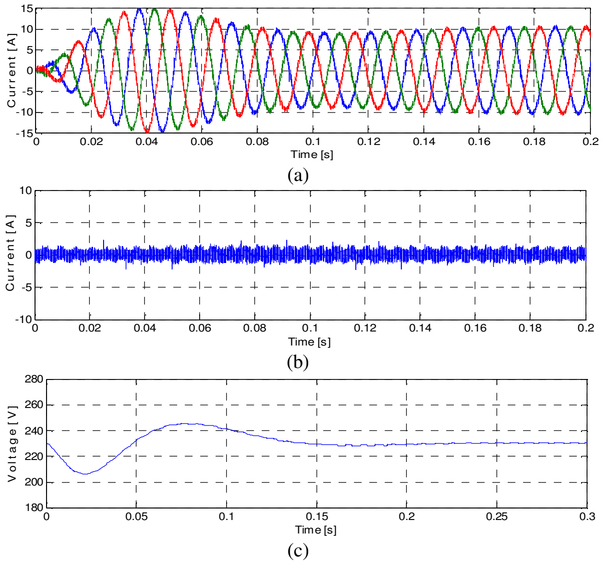

Fig. 13. 3F-B topology: (a) i_{sa}, i_{sb} and i_{sc}, (b) i_{sn}; (c) V_{dc}.

Table II shows the total harmonic distortion (THD) obtained in the three-phase source currents, after the current compensation for both topologies.

Table II - Total Harmonic Distortion of the Source Currents.

THD%	phase *a*	phase *b*	phase *c*
Without compensation	42.09	39.97	36.10
F-L compensation	1.72	1.24	1.06
3F-B compensation	1.51	1.59	1.17

As the 3F-B topology can control each phase independently, by means of the SRF-based algorithm shown in Fig. 4, only harmonic suppression and reactive compensation are performed, thus the unbalance load compensation is not taken into account. For this condition, Fig. 14 shows the compensated source currents (i_{sa}, i_{sb}, i_{sc}), the neutral current (i_{sn}) and the dc-bus voltage (V_{dc}). As can be noted, the input currents are unbalanced, although harmonic free.

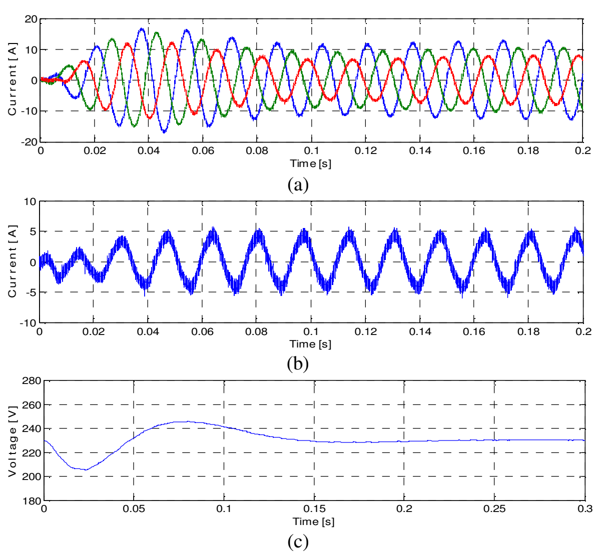

Fig. 14. 3F-B topology: (a) i_{sa}, i_{sb} and i_{sc}, (b) i_{sn}; (c) V_{dc}.

5. Conclusion

This work presented a study of two shunt APF topologies, such as the F-L and the 3F-B. They were applied for harmonic current suppression, reactive power compensation and/or load unbalanced compensation in three-phase four-wire systems. The SRF-based algorithms used to extract the reference currents were presented. The F-L topology, performed into $\alpha\beta 0$-axes, was implemented using SVM. Through the modeled plant, the PI controllers for F-L topology were set in synchronous frame, allowing the elimination of the steady-state errors. Although the 3F-B APF uses additional switches and isolation transformers, when it is compared with F-L APF, it requires lower dc-bus voltage and is able to control each phase independently. Mathematical analyses of these two topologies were developed in order to obtain a linear model that represents the physical system, allowing to set the gains of PI current controllers. The simulation results were presented to evaluate the performance of the shunt APFs approaches.

Acknowledgement

The authors gratefully acknowledge the financial support received from CNPq, process n° 471825/2009-3, and from Araucária Foundation, process n° 06/56093-3.

References

[1] T. M. Gruzs, "A survey of neutral currents in three-phase computer power systems", IEEE Trans. on Industry Applications, vol. 26, no. 4, pp. 719-725, July/Aug. 1990.

[2] P. Salmerón, S. P. Litrán, R. S. Herrera and J. R. Vázquez, "A Pratical Comparative Evaluation of Different Active Harmonic Filter", in Proc. of ICREPQ'11 , paper 230, 2010.

[3] B. Singh, K. A. Haddad and A. Chandra, "A Review of Active Filters for Power Quality Improvement", IEEE Trans. on Industrial Electronics, vol. 46, no. 5, pp. 960-971, October 1999.

[4] N. Mendalek, "Modeling and Control of Three-Phase Four-Leg Split-Capacitor Shunt Active Power Filter", in Proc. of ACTEA, pp. 121-126, 2009.

[5] R. Pregitzer, J.G. Pinto, L.F.C. Monteiro and J.L. Afonso, "Shunt Active Power Filter with Dynamic Output Current Limitation", in Proc. of ISIE, pp. 1021-1026, 2007.

[6] I. Z. Abdalla, K. S. Rama Rao and N. Perumal, "Three-Phase Four-Leg Shunt Active Power Filter to Compensate Harmonics and Reactive Power", in Proc. of ISCI, pp. 20-22, 2011.

[7] V. Khadkikar and A. Chandra, "An Independent Control Approach for Three-Phase Four-Wire Shunt Active Filter Based on Three H-Bridge Topology under Unbalanced Load Conditions", in Proc. of PESC, pp. 4643-4649, 2008.

[8] S. Srianthumrong, H. Fujita and H. Akagi, "Stability Analysis of a Series Active Filter Integrated With a Double-Series Diode Rectifier", IEEE Transactions on Power Electronics, vol. 17, no. 1, pp. 117-124, January 2002.

[9] C. L. Chen, C. E. Lin and C. L. Huang, "An Active Filter for Unbalanced Three-Phase System Using Synchronous Detection Method", in Proc. of PESC , vol. 02, pp. 1451-1455, 1994.

[10] S. A. O. da Silva and R. A. Modesto, "A Comparative Analysis of SRF-based Controllers Applied to Active Power Line Conditioners", in Proc. of IECON, pp. 405-410, 2003.

[11] A. Kouzou, M. O. Mahmoudi and M. S. Boucherit, "A New 3D-SVPWM Algorithm for Four-Leg Inverters", in Proc. of IEMDC , pp. 1674-1681, 2009.

[12] H. Pinheiro, F. Botterón, C. Rech, L. Schuch, R.F. Camargo, H.L. Hey, H.A. Gründling and J.R. Pinheiro, "Space Vector Modulation for Voltage-Source Inverters: A Unified Approach", in Proc. of IECON, vol. 01, pp. 23-29, 2002.